Synthesis and characterization of MnS$_2$/reduced graphene oxide nanohybrid: an efficient adsorbent for pharmaceutical compound removal

Ali Fakhri[a],*, Sahar Rashidi[b], Mohammad Asif[c],*, Ahmed A. Ibrahim[d]

[a]Young Researchers and Elites Club, Science and Research Branch, Islamic Azad University, Tehran, Iran, Tel. +98 9124271296,
email: ali.fakhri88@yahoo.com (A. Fakhri)
[b]Department of Chemical Engineering, South Tehran Branch, Islamic Azad University, Tehran, Iran,
email: srashidi05@gmail.com (S. Rashidi)
[c]Department of Chemical Engineering, King Saud University, Riyadh, Saudi Arabia, Tel. +966114676849,
email: masif@ksu.edu.sa (M. Asif)
[d]Department of Chemical Engineering, King Saud University, Riyadh, Saudi Arabia, email: aidid@ksu.edu.sa (A.A. Ibrahim)

ABSTRACT

The increasing use of pharmaceuticals is causing serious environmental pollution because of their improper disposal, leading to water contamination. Of particular concern are benzodiazepines (BDZs) given their low removal efficiencies by conventional treatment processes. This concern warrants the development of alternative or complementary treatment technologies with high removal efficiencies. Toward this end, we have developed a facile one-step hydrothermal method to synthesize a nanohybrid of manganese sulfide (MnS$_2$) and reduced graphene oxide for the efficient adsorptive removal of the most commonly detected BDZ, that is, alprazolam (ALP). The as-prepared samples were thoroughly characterized using X-ray diffraction, field emission scanning electron microscopy, transmission electron microscopy, ultraviolet-visible (UV-Vis) absorption spectroscopy, and photoluminescence spectroscopy. Removal of ALP from aqueous solutions was investigated at different temperatures, pH values, and adsorbent dosages. Both high pH and temperature favored ALP removal. The experimental equilibrium data could be accurately described by the Langmuir isotherm model, whereas the adsorption kinetic data were well-represented by the pseudo-second-order model. Relevant thermodynamic parameters, such as Gibbs free energy ($\Delta G°$), enthalpy change ($\Delta H°$), and entropy change ($\Delta S°$), were also calculated from the experimental equilibrium data. The positive value of $\Delta H°$ and the negative value of $\Delta G°$ indicated the endothermic and spontaneous nature of ALP adsorption by the synthesized adsorbent. Multiple adsorption–desorption cycles indicated that the present adsorbent can be efficiently regenerated several times without significant degradation in its performance.

Keywords: Reduced graphene oxide; Alprazolam; Adsorption equilibrium; Kinetics; Thermodynamics

1. Introduction

The increasing use of pharmaceutical compounds has caused increasing global environmental concern because wastes containing such compounds often contaminate the aquatic environment through direct and indirect disposal methods [1–4]. Benzodiazepines (BDZs) are among the most prescribed groups of pharmaceuticals worldwide. Their prescription is also common in veterinary treatments for anxiolytic and appetite stimulation effects. The improper disposal of these pharmaceuticals could lead to water contamination, which can cause mutagenic and carcinogenic effects on human and animals. Several studies reported the occurrence of BDZs in environmental matrices, including drinking water, and in influents and effluents of wastewater treatment plants. The most frequently

*Corresponding author.

detected BDZs include alprazolam (ALP), which is commonly used to treat anxiety and panic disorders [5,6]. The chemical and physical characteristics of ALP are summarized in Table 1.

A recent study has reported the photodegradation efficiency of four BDZs, namely, lorazepam, oxazepam, diazepam, and ALP [7]. The half-lives of lorazepam, oxazepam, and diazepam were found to be 1, 4, and 7 sunny summer days, respectively; ALP displayed an exceptionally high resistance to photodegradation, with a half-life of 228 d [7]. Therefore, photodegradation is ineffective in preventing the ALP contamination of the aquatic environment. Another recent study demonstrated the extremely low removal efficiencies (less than 25%) of two wastewater treatment plants in New York for some pharmaceuticals, including ALP [8]. Consequently, further studies were recommended for limiting the amount of such pharmaceutical contaminants in the receiving water. Tomic et al. [9] synthesized brookite-type titania (titanium dioxide, TiO_2) nanopowders using the sol–gel hydrothermal method under different temperature and hydrothermal reaction conditions and investigated their effectiveness for the photocatalytic degradation of ALP under UV light irradiation. Their study focused on the optimization of titania nanopowder synthesis to enhance the removal rate of ALP from the water suspension. The sample synthesized at 200°C with 24 h hydrothermal reaction time was the most effective, removing 98% ALP during 30 min of contact with the aqueous phase. The degradation kinetics was well-represented by the pseudo-first-order kinetic model. At a relatively high initial ALP concentration of 0.03 mM (9.3 mg/L), the first-order rate constants (for the first 10 min of irradiation) of samples were 0.034, 0.179, and 0.077 per minute after 12, 24, and 48 h of hydrothermal reaction, respectively [9].

These studies clearly emphasize the need to develop and implement cost-effective and efficient separation techniques for mitigating the accumulation and persistence of pharmaceutical compounds in the environment [10]. Adsorptive treatment methods are ideally suited to address pharmaceutical contamination issues, which mostly involve low contaminant concentrations in water [11]. The development of a novel adsorptive material featuring high uptake amount and rate is the key challenge. Semiconductor metal sulfide (e.g., ZnS and MnS_2) nanoparticles (NPs) have been extensively investigated because of their unique properties and potential application in diverse areas, including photocatalysis, solar cells, display panels, and new devices such as single electron transistors [12–14]. MnS_2 has a wide band gap energy of Eg (T = 0) ~ 3.7 eV and occurs in three forms: a stable green α-MnS with a rock-salt-type structure and two pink metastable tetrahedral structures, β-MnS_2 (sphalerite type) and γ-MnS_2 (wurtzite type) [15]. Another recently discovered material, graphene, has attracted considerable attention because of its unique properties and large specific surface area. A combination of both materials could potentially be an effective nanohybrid adsorbent given graphene's uniquely high mechanical strength that can help stabilize the structure of the adsorbent and provide a 2D plane for contaminant deposition [16]. Transport through delocalized conjugated π structures allows charge carriers in graphene to achieve high mobility and relatively slow charge recombination. In the present study, a novel nanohybrid adsorbent, MnS_2/reduced graphene oxide (r-GO), was synthesized and then characterized. The effectiveness of the present adsorbent for ALP removal was investigated. Considering that the ALP concentration in the aquatic environment is often very low, the present investigation, unlike previous studies, maintained a low initial ALP concentration. The influences of key variables, including reaction temperature and solution pH, on the uptake efficiency of the nanohybrid adsorbent were examined. The effect of the optimum adsorbent dosage was also investigated. The progress of the adsorption reaction was monitored with time at different temperatures to determine the rate of pharmaceutical uptake. The kinetic data obtained were fitted with different kinetic models to determine their suitability to predict the removal rate of ALP with the synthesized nanohybrid adsorbent. Experimental equilibrium data were also fitted with various adsorption isotherm models to compute their parameters and determine the isotherm that best describes the experimental data. Thermodynamic parameters of interest that characterize the adsorption of ALP on MnS_2/r-GO were computed.

2. Materials and methods

2.1. Preparation of MnS$_2$/r-GO nanohybrid

Raw materials used in this study were procured from Sigma–Aldrich, Ltd. Graphene oxide (GO) nanosheets were synthesized using the modified Hummer's method as previously described [9]. A MnS_2/r-GO nanohybrid sample was prepared by a simple one-step hydrothermal method. In a particular experiment, 1 mmol $MnCl_2 \cdot 4H_2O$ was added to 60 mL of aqueous GO dispersion (1.5 mg GO mL^{-1}) under continuous stirring at room temperature. After 1 h, 2 mmol thiourea was added, and the mixture was stirred for another 40 min. Subsequently, the mixture was transferred into a Teflon-lined stainless steel autoclave and heated at 180°C for 12 h. After cooling to room temperature, the precipitates were collected by centrifugation, washed with deionized water, and then dried at 60°C for 12 h in a vacuum to obtain the final product.

2.2. Materials characterization

The morphology of the synthesized adsorbent was examined using field emission scanning electron microscopy (FESEM-Hitachi SU8000) and X-ray diffractometer (XRD, Philips X'Pert). The particle size of the MnS_2/r-GO

Table 1
Physiochemical properties of ALP

Molecular weight (g mol^{-1})	Melting point (°C)	Chemical structure
308.765	228–228.5	
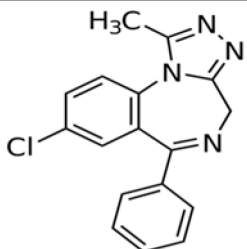
nanohybrid was measured under a transmission electron microscope (TEM, Zeiss EM-900). The Brunauer–Emmett–Teller surface area of the MnS_2/r-GO nanohybrid was measured using the Micromeritics ASAP2020. Ultraviolet-visible (UV–Vis) and photoluminescence studies were performed using the TEC Avaspec 2048 Spectrophotometer (excitation source = Xenon arc lamp 450 W). The ζ-potentials were measured with a PenKem Lazer Zee model 501 apparatus.

2.3. Experimental methods

To determine the optimum values of critical adsorption parameters, several adsorption experiments were carried out in batch mode by varying only the parameter of interest under study and keeping all other parameters constant. Various ALP solution concentrations (0.1–0.6 mg/L) were used. The adsorbent dosage range was 0.10–1.00 g/L, and the pH varied from 2 to 10. ALP concentration was measured through 2D gas chromatography (Kimia Shangarf Pars Research Co., Iran). The equilibrium adsorption capacity (q_e), that is, the amount of ALP adsorbed per unit weight (mg/g) of the adsorbent (MnS_2/r-GO nanohybrid), was evaluated as follows:

$$q_e = \left(C_0 - C_e\right)\left(\frac{V}{m}\right), \tag{1}$$

where C_o and C_e are the initial and final equilibrium concentrations of ALP in mg/L, respectively; V is the volume of solution in L; and m is the adsorbent mass in mg.

2.4. Desorption experiments

HNO_3 (0.1 M) was used as the elution reagent. Initially, 100 mg of the adsorbent was weighed and dissolved in 50 mL of HNO_3 solution. The mixture was placed in an ultrasonic cleaner, KS-300EI. Three runs with identical conditions were carried out for each experiment. The reproducibility of the experimental data was within ±3%.

2.5. Adsorbent regeneration experiments

Repeated batch adsorption–desorption experiments were conducted to determine the reusability of the nanohybrid adsorbent. After the first adsorption experiment, the adsorbent was washed with deionized water to remove the traces of acid and then dried in a vacuum oven at 70°C before use for the second adsorption experiment. This procedure was repeated again for the next adsorption–desorption experiment. Five consecutive cycles were carried out using the same adsorbent.

3. Results and discussion

3.1. Characterization of the MnS_2/r-GO nanohybrid

3.1.1. XRD patterns

According to the XRD patterns presented in Fig. 1. GO showed a sharp diffraction peak at $2\theta = 10.8°$, thereby suggesting the complete removal of graphite [17]. When GO was hydrothermally treated in the presence of thiourea, the (002) diffraction peak completely disappeared, whereas a broad
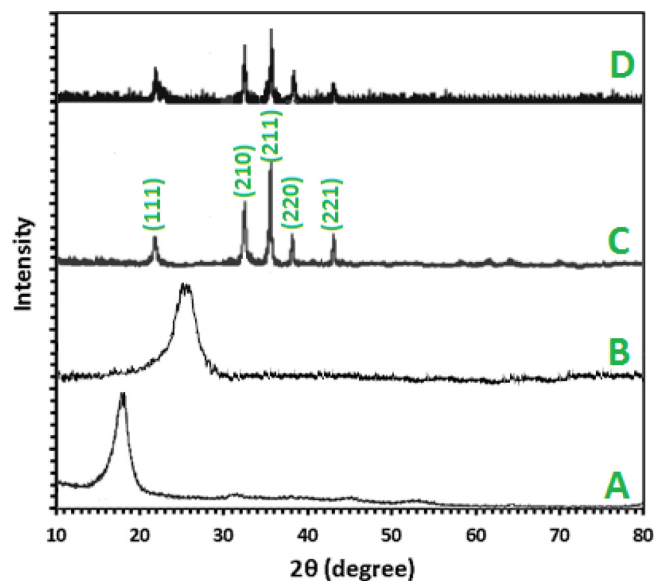
Fig. 1. XRD patterns of the prepared GO (A), r-GO (B), MnS_2 (C), and MnS_2/r-GO (D) samples.

diffraction peak emerged at $2\theta = 24.5°$. Thiourea acted as a reducing agent at elevated temperature under hydrothermal conditions. Therefore, the hydrothermal reaction between $MnCl_2$ and thiourea resulted in the formation of pure cubic crystalline structure MnS_2 (JCPDS card No. 25-0549) with d-spacing values of 3.06, 2.72, and 1.66Å. Hydrothermal treatment of the mixture of GO, $MnCl_2$, and thiourea led to the simultaneous reduction of GO and formation of MnS_2.

3.1.2. Morphology and structure

The representative SEM and TEM images of r-GO, MnS_2, and the MnS_2/r-GO nanohybrid are shown in Fig. 2. As shown in Fig. 2A and 2B, the layers of the r-GO sheets are structured, irregular, and folding, and the single- or few-layer r-GO nanosheets contain many wrinkles. Fig. 2C and 2D indicate the surface structure and morphology of the MnS_2 NPs. Spherical- to ellipsoid-shaped particles were formed. The size of the MnS_2 NPs varies in the range of 20–30 nm. Fig. 2E shows that a large amount of the MnS_2 NPs is embedded into the interlayer of r-GO sheets. Fig. 2F illustrates that the r-GO sheets are decorated by the MnS_2 NPs. The r-GO sheets act as bridges for the connection between different MnS_2 NPs. The nitrogen adsorption and desorption isotherms for pure MnS_2 and the MnS_2/r-GO nanohybrid were evaluated. The total pore volumes of pure MnS_2 and the MnS_2/r-GO nanohybrid were 0.540 and 1.173 cm^3/g, respectively. The specific surface areas of pure MnS_2 and the MnS_2/r-GO hybrid were 45.91 and 98.23 m^2/g, respectively. Thus, the nanohybrid formation increased the pore volume and surface area of the adsorbent by more than 100%.

3.1.3. Optical properties

We examined the optical properties of both pure MnS_2 and the MnS_2/r-GO nanohybrid by analyzing the photoluminescence spectra and UV–Vis spectra. The MnS_2 NPs dis-
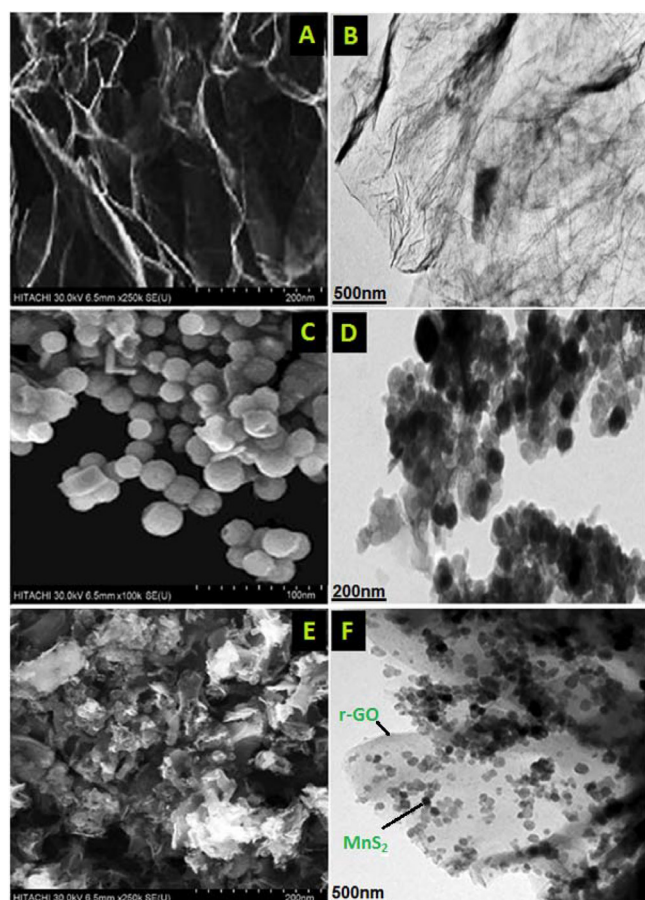
Fig. 2. FE-SEM and TEM images of the r-GO (A,B), MnS$_2$ (C,D), and MnS$_2$/r-GO (E,F) samples.

play an excitonic absorption peak in the UV region with a band gap absorption edge at 356 nm (Fig. 3A) because of the electron transition from the valence band to the conduction band [18,19]. The presence of r-GO substantially increased the absorption of light in the visible region between 400 and 800 nm for the MnS$_2$/r-GO nanohybrid. As shown in Fig. 3B, the PL spectra of pure MnS$_2$ NPs are asymmetrical and can be decomposed into different peaks centered at 400, 430, and 448 nm; a strong broad peak with a wavelength range between 460 and 480 nm may be attributed to surface defects and vacancies [19]. By contrast, the PL spectra of the MnS$_2$/r-GO nanohybrid are similar to those of the MnS$_2$ NPs but are quenched in the MnS$_2$/r-GO nanohybrid because of the interaction of the MnS$_2$
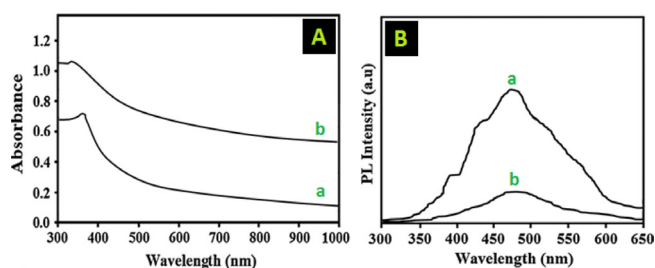
Fig. 3. UV–Vis absorbance (A) and PL spectra (B) of the MnS$_2$ (a) and MnS$_2$/r-GO (b) samples.

surface with r-GO, thereby increasing the photo-generated electron transfer from the MnS$_2$ NPs to r-GO.

3.2. Adsorption study

The effect of reaction time was first studied in this work at different temperatures (Fig. 4). The removal rate was initially fast and then gradually decreased with time. During the first 12 min of contact, the amount of ALP removal increased linearly with time, gradually decreased, and then reached equilibrium after 20 min. The removal efficiency (endothermic reaction) improved with increasing temperature because of the fast diffusion of ALP molecules inside the matrix of the MnS$_2$/r-GO nanohybrid at high temperatures.

Solution pH is a key variable significantly affecting the removal of pharmaceuticals. In the present investigation, ALP removal was studied over a wide range of pH (Fig. 5). The adsorption of ALP increased with increasing pH from 3 to 8.5. Beyond this pH level, the adsorbent hardly showed
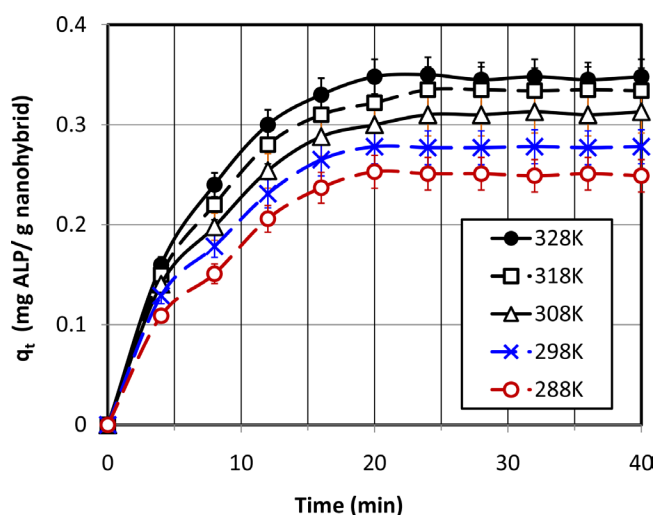
Fig. 4. Effect of temperature and contact time on the ALP removal (Initial ALP concentration = 0.4 mg/L; Adsorbent dose = 0.4 g/L; pH= 8.5).
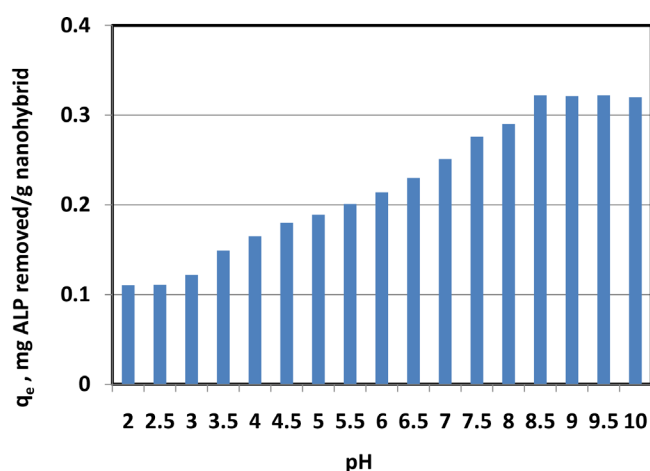
Fig. 5. Influence of pH on the ALP removal efficiency (Initial ALP concentration = 0.4 mg/L; Adsorbent dose = 0.4 g/L; Contact time = 20 min; T = 318 K).

any improvement in the contaminant uptake. This result indicates that the charge on the surface of the MnS_2/r-GO nanohybrid remains positive for a wide range of pH. The isoelectric points [pH(I)] of MnS_2 with NaCl-supported electrolyte solutions were evaluated to be between pH 3.3 and 0.6. The metal sulfide surfaces were positively charged below pH(I) while negatively charged above pH(I). The increase in ALP adsorption with increasing pH demonstrates the presence of an electrostatic attraction between the negative charge of the MnS_2/r-GO nanohybrid and the positive charge of ALP.

The effect of adsorbent dose on the removal efficiency of ALP was investigated by keeping the solution concentration fixed at 0.4 mg/L. As shown in Fig. 6 different adsorbent dosages (0.2–1 g/L) were used. The removal of ALP was enhanced with increasing adsorbent amount. The amount of ALP adsorbed from aqueous solution peaked at 0.4 g/L of adsorbent.

3.2.1. Investigation of adsorption isotherms, kinetics, and thermodynamics

The uptake capacity of adsorbents is a function of equilibrium concentration. Different isotherm models can be used to represent adsorption isotherm data. For example, the Langmuir isotherm model assumes that the maximum removal is related to a monolayer saturated with molecules of adsorbate on the surface of the adsorbent, which is energetically homogeneous. The linear form of the Langmuir model is given as [20,21]

$$\left(\frac{1}{q_e}\right) = \frac{1}{bQ}\left(\frac{1}{C_e}\right) + \frac{1}{Q} \tag{2}$$

where Q is the maximum adsorption capacity (mg/g) and b is the energy of adsorption. Another well-known Freundlich isotherm model assumes multilayer adsorption on a heterogeneous surface with an exponential distribution of active sites [22]. This model is given as

$$q_e = K_F C_e^{\frac{1}{n}} \tag{3}$$
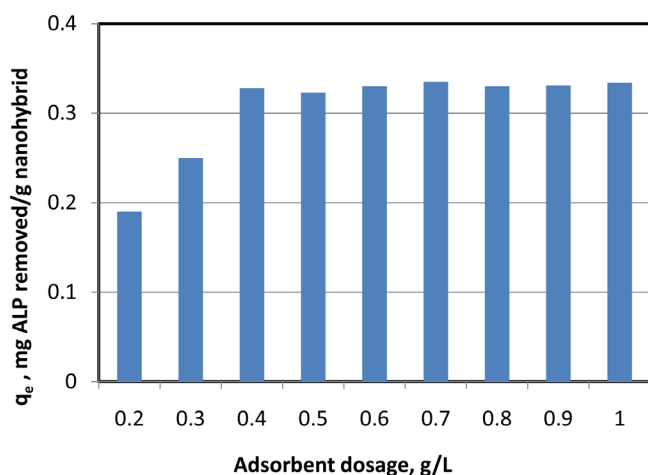
Fig. 6. Influence of adsorbent mass on the removal of ALP (Initial ALP concentration = 0.4 mg/L; Contact time = 20 min; pH = 8.5; T = 318 K).

where K_F is the adsorption capacity (mg/g), and n is a measure of surface heterogeneity or adsorption intensity. Conversely, the Temkin isotherm model assumes that the heat of adsorption decreases linearly with increasing coverage [23,24]. The linear form of the Temkin isotherm model is given as

$$q_e = B_T \ln C_e + B_T \ln K_T \tag{4}$$

where B_T and K_T are constants that can be determined from the plots of q_e and C_e.

Fig. 7 shows the comparison between the experimental equilibrium adsorption data and the three isotherm models discussed above. Model equations and their correlation coefficients (R^2) are also shown in the figure. The slopes, intercept, and associated standard errors for different isotherm models are presented in Table 2a. Relevant isotherm parameters are summarized in Table 2b. The R^2 values, which is a measure of goodness-of-fit, clearly indicates that the ALP adsorption onto the MnS_2/r-GO nanohybrid is best represented by the Langmuir isotherm. This observation is also evident in Fig. 7d, where the predictions of all the three isotherm models are compared with the experimental data

The kinetic data of ALP adsorption onto the MnS_2/r-GO nanohybrid were also analyzed using different kinetic models. The pseudo-first-order kinetic model can be written as [25]

$$ln\left(\frac{q_e - q_t}{q_e}\right) = -k_1 t \tag{5}$$

where q_e is the equilibrium amount of adsorbate (mg) per unit mass (g) of the adsorbent, q_t is the adsorbed amount at any time t, and k_1 is the first-order rate constant (1/min). The linearized pseudo-second-order adsorption kinetic model is given as [25]

$$\frac{t}{q_t} = \frac{t}{q_e} + \frac{1}{k_2 q_e^2} \tag{6}$$

where k_2 is the rate constant for the pseudo-second-order model (g/mg min). The adsorption of the contaminant involves mass transfer from the bulk solution to the interior sites of the adsorbent. Thus, two mass transport resistances control the contaminant movement: internal mass transport resistance due to the intraparticle diffusion governing the movement of the contaminant inside the pores of the adsorbent and the external mass transport resistance due to the liquid film between the adsorbent and the bulk solution. The intraparticle diffusion model is given as [26]

$$q_t = K_i t^{\frac{1}{2}} + C \tag{7}$$

where C is the adsorption constant, and K_i is the intraparticle diffusion rate constant (mg/g·min$^{0.5}$).

The best-fit parameters for the aforementioned models are presented in Table 3. Higher R^2 value indicate that the pseudo-second-order kinetic model is capable of accurately. describing the the adsorption process. Note that standard errors in estimation of the slope and the intercept of the second order model are 0.0619 and 0.6780, respectively. Experimental data and model predictions are presented in
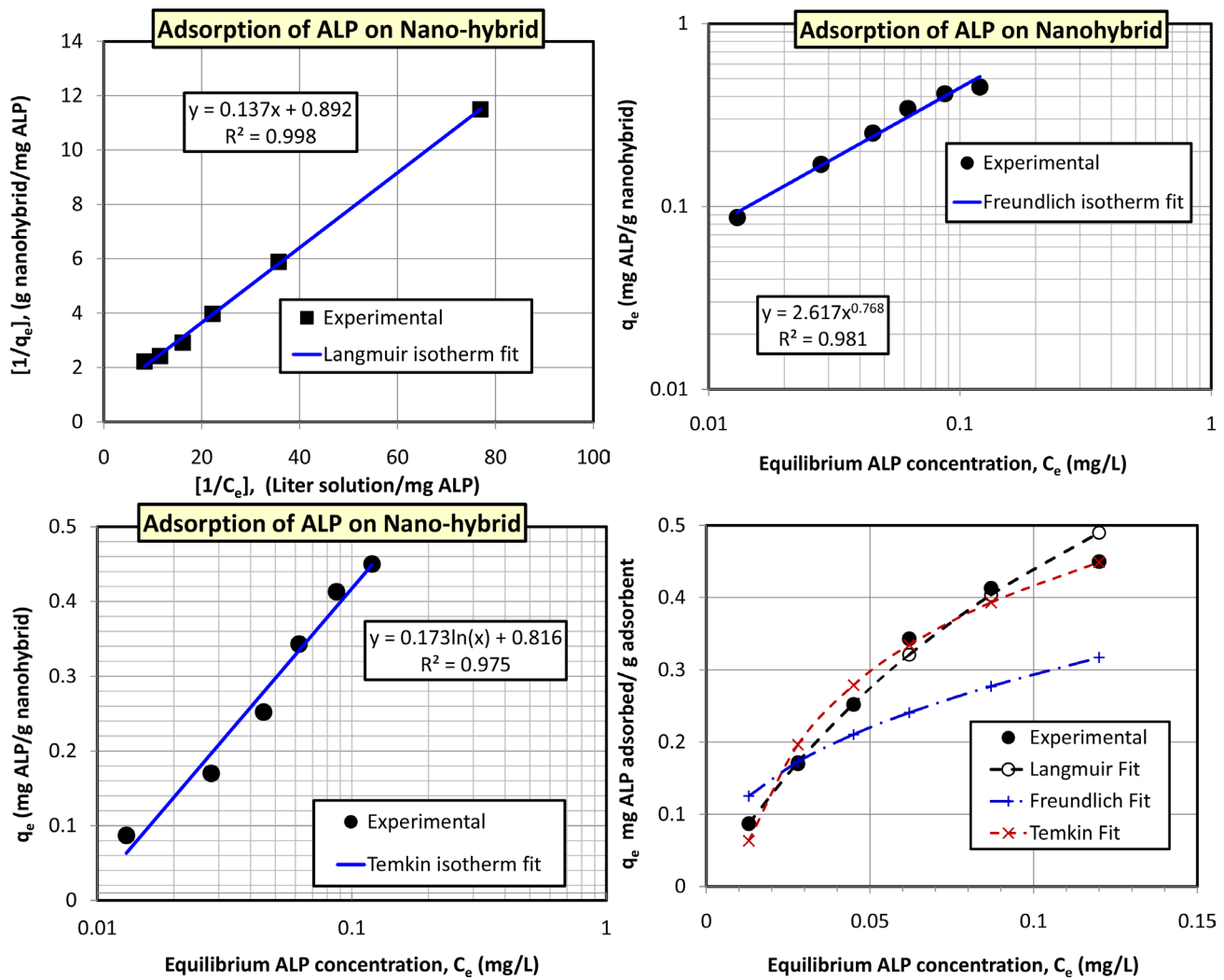
Fig. 7. Predictions of equilibrium isotherm models for adsorption of ALP onto MnS2/r-GO nanohybrid for Initial ALP concentration = 0.4 mg/L, Adsorbent dose = 0.4 g/L, pH = 8.5; T = 328 K (a) Langmuir isotherm fit; (b) Freundlich isotherm fit; (c) Temkin isotherm; (d) Comparison.

Fig. 8. The predictions of pseudo-second-order kinetics are superior while the intraparticle mass transport governs the movement of ALP inside the nanohybrid adsorbent developed in the present study [27] .

The rate data were further investigated by the method given by Reichenberg, using Eqs. (8)–(10), as follows [28] :

$$\ln(1-F) = -Bt \tag{8}$$

$$F = \frac{q_t}{q_e} \tag{9}$$

$$B = \frac{\pi^2 D_i}{r_0^2} \tag{10}$$

Table 2a
Estimation of slopes, intercepts, and standard errors for different isotherm models

Isotherm model	Slope		Intercept		R^2
	Mean	Std Error	Mean	Std Error	
Langmuir	0.1379	0.0025	0.8921	0.0913	0.9987
Freundlich	0.7688	0.0522	0.4178	0.0714	0.9819
Temkin	0.1735	0.0137	0.8169	0.0431	0.9757

Table 2b
Isotherm parameters for ALP adsorption onto MnS_2/r-GO nanohybrid

Langmuir isotherm		Freundlich isotherm		Temkin isotherm	
Q (mg/g)	B (L/mg)	n	K_F (mg/g)	B_T	K_T (L/mg)
1.121	6.469	1.301	2.617	0.1735	110.82

Table 3
Parameters of kinetic models for ALP adsorption on MnS$_2$/r-GO nanohybrid

Parameters	Mean values
Pseudo-first-order	
q_e (mg/g)	0.4673
k_1 (1/min)	0.1996
R^2	0.9841
Pseudo-second-order	
q_e (mg/g)	0.5187
k_2 (g /mg min)	1.928
R^2	0.9979
Intraparticle diffusion	
K_i (mg/g min$^{0.5}$)	0.0867
C	−0.0089
R^2	0.9900
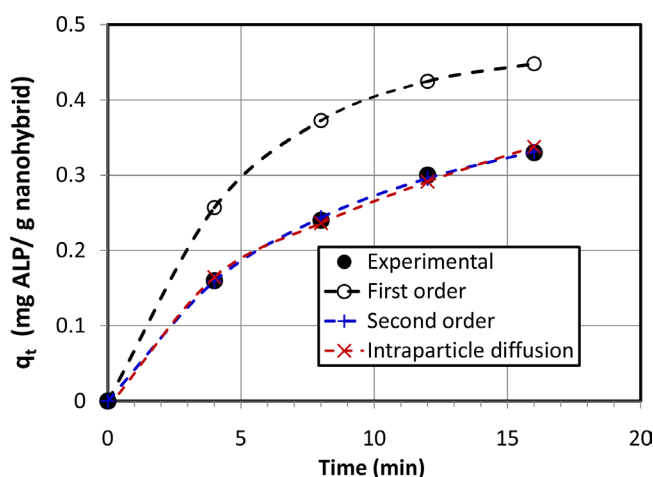
Fig. 8 Comparison of prediction of kinetic models for the adsorption of alprazolam on MnS$_2$/r-GO nanohybrid (Initial ALP concentration = 0.4 mg/L; Adsorbent dose = 0.4 g/L; pH = 8.5; T = 328 K).

where, B is the time permanent, D_i is the effective diffusion coefficient of the ALP molecule in the adsorbent phase, F is the fractional acquisition of equilibrium at time t, and r_0 is the radius of the adsorbent particle. The plot of ln $(1 − F)$ versus t yields the value of B as the slope of the straight line. The model parameters and R^2 are presented in Table 4. The intercept in Eq. (8) is zero.

Thermodynamic considerations of the removal mechanism are important to understand the nature of the reaction. The experimental data evaluated at different temperatures were used to compute the thermodynamic parameters $\Delta G°$, $\Delta H°$, and $\Delta S°$. $\Delta G°$ is given by the following equations [29]:

$$\Delta G^0 = -RTlnK_L \tag{11}$$

$$\Delta G^0 = \Delta H^0 - T\Delta S^0. \tag{12}$$

Table 4
Effective diffusion coefficient for ALP transport

Film diffusion mass transfer rate	ALP
B	0.0759
D_i (m^2/s)	3.570×10^{-6}
R^2	0.966

$\Delta S°$ and $\Delta H°$ were computed from the intercept and slope of the plot $\Delta G°$ vs. temperature T (figure not shown). The computed values are reported in Table 5. The $\Delta H°$ value is positive, thereby indicating that the ALP removal reaction is endothermic. The negative $\Delta G°$ values confirm the spontaneous nature of ALP removal by the MnS$_2$/r-GO nanohybrid. The $\Delta S°$ positive value reflects an enhancement of the condition on the solid/liquid interface before the adsorption reaction [29]

3.3. Comparison

Tomic et al. [9] has recently analyzed the photo-catalytic degradation of ALP using three types of brookite-type titania nanopowder. This work focused on the optimization of synthesis parameters to improve the uptake rate of ALP. Both temperature and hydrothermal reaction time critically affected the performance of the catalyst samples. The sample synthesized at 200°C with 24 h of hydrothermal reaction yielded the highest removal rate of ALP with a first-order rate constant of 0.179/min. On the other hand, samples prepared with 12 and 48 h of hydrothermal reaction showed much slower reaction rates, with the first-order rate constants being 0.034/min and 0.077/min, respectively [9]. In the present study, higher rate constants of 0.2/min and 0.24 g/mg min were obtained despite the lack of attempt to optimize the synthesis parameters for the prepared nanohybrid adsorbent.

3.4. Performance evaluation

The performance of the nanohybrid adsorbent was evaluated by carrying out five consecutive adsorption–desorption cycles using the same batch of adsorbent. The effects of time on the desorption dynamics was initially studied (Fig. 9). The desorption capacity of the MnS$_2$/r-GO nanohybrid initially increased, reaching a maximum after approximately 20 min of contact. Prolonging the contact time decreased the desorption capacity of the nanohybrid. This phenomenon is apparently caused by the generation of holes because of ultrasonication [30,31]. The reusability

Table 5
Thermodynamic parameters for adsorption of ALP on MnS$_2$/r-GO nanohybrid

$\Delta H°$ (KJ mol^{-1})	$\Delta S°$ (J mol^{-1} K^{-1})	$\Delta G°$ (KJ mol^{-1})				
		288 K	298 K	308 K	318 K	328 K
13.94	59.02	−3.109	−3.642	−4.232	−4.822	−5.412
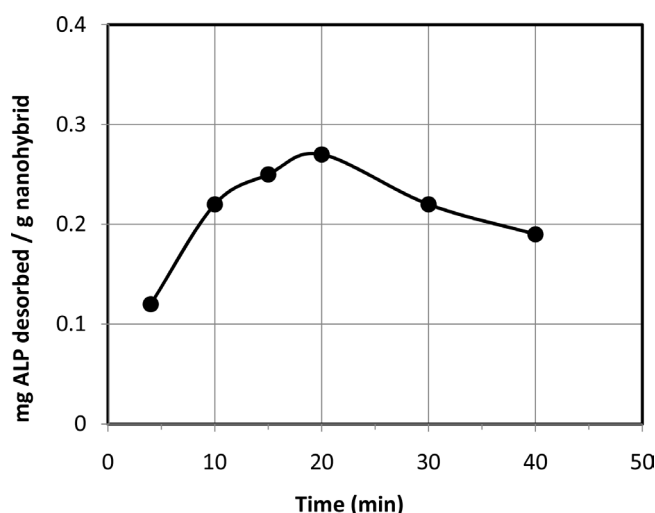
Fig. 9. Desorption dynamics of MnS$_2$/r-GO nanohybrid at T = 328K.

Table 6
Performance evaluation of MnS$_2$/r-GO nanohybrid during adsorption/desorption experiments

Regeneration Cycles	1st	2nd	3rd	4th	5th
Adsorption (mg/g)	0.34	0.32	0.30	0.28	0.24
Desorption (mg/g)	0.27	0.25	0.22	0.19	0.15

of the nanohybrid was investigated in multiple adsorption–desorption cycles (6). As seen in Table 6, there was a gradual but insignificant decrease in the adsorption capacity in the first four cycles. An 18% decrease in the overall adsorption capacity was observed after the four cycles of reuse. However, in the fifth cycle, a relatively greater performance deterioration was evident. Therefore, the MnS$_2$/r-GO nanohybrid exhibits potential applications as an efficient, inexpensive, and recyclable adsorbent for the treatment of pharmaceutical-contaminated wastewater.

4. Conclusions

A MnS$_2$/r-GO nanohybrid was successfully synthesized and characterized using a simple one-pot hydrothermal method. The ALP adsorption from aqueous solution using the MnS$_2$/r-GO nanohybrid adsorbent was investigated. The removal of ALP improved with increasing pH and temperature. The pseudo-second-order model was found suitable for explaining the experimental adsorption kinetic data. Experimental adsorption isotherm data were fitted using different isotherm models. The Langmuir isotherm model best represented the experimental data. The adsorption thermodynamics of ALP was also investigated, and the values of $\Delta G°$, $\Delta S°$, and $\Delta H°$ were computed. The ALP adsorption by the MnS$_2$/r-GO nanohybrid was spontaneous and endothermic. Multiple adsorption–desorption cycles indicated that the present adsorbent can be efficiently regenerated several times without significant degradation in its performance. It is evident from multiple cycles of adsorption-desorption that the present adsorbent can be efficiently regenerated without any significant performance degradation. In fact, no significant degradation of adsorbent performance was noticed for the first 4 cycles of adsorption-desorption experiments.

References

[1] Z. Dong, D.B. Senn, R.E. Moran, J.P. Shine, Prioritizing environmental risk of prescription pharmaceuticals, Regul. Toxicol. Pharm., 65 (2013) 60–67.
[2] K. Fent, A.A. Weston, D. Caminada, Ecotoxicology of human pharmaceuticals, Aquat. Toxicol., 76 (2006) 122–159.
[3] T. Kosjek, S. Perko, M. Zupanc, M. Zanoški Hren, T. Landeka Dragičević, D. Žigon, B. Kompare, E. Heath, Environmental occurrence, fate and transformation of benzodiazepines in water treatment, Water Res., 46 (2012) 355–368.
[4] D.R. Baker, B. Kasprzyk-Hordern, Spatial and temporal occurrence of pharmaceuticals and illicit drugs in the aqueous environment and during wastewater treatment: New developments, Sci. Total Environ., 454–455 (2013) 442–456.
[5] G.W. Dawson, S.G. Jue, R.N. Brogden, Alprazolam: A review of its pharmacodynamic properties and efficacy in the treatment of anxiety and depression, Drugs, 27 (1984) 132–147.
[6] S. Maitra, B. Saha, C.R. Santra, A. Mukherjee, S. Goswami, P.K. Chanda, P. Karmakar, Alprazolam induced conformational change in hemoglobin, Int. J. Biol. Macromol., 41 (2007) 23–29.
[7] V. Calisto, M.R.M. Domingues, V.I. Esteves, Photodegradation of psychiatric pharmaceuticals in aquatic environments – kinetics and photodegradation products, Water Res., 45 (2011) 6097–6106.
[8] B. Subedi, K. Kannan, Occurrence and fate of select psychoactive pharmaceuticals and antihypertensives in two wastewater treatment plants in new york state, USA, Sci. Total Environ., 514 (2015) 273–280.
[9] N. Tomić, M. Grujić-Brojčin, N. Finčur, B. Abramović, B. Simović, J. Krstić, B. Matović, M. Šćepanović, Photocatalytic degradation of alprazolam in water suspension of brookite type tio2 nanopowders prepared using hydrothermal route, Mater. Chem. Phys., 163 (2015) 518–528.
[10] O.A.H. Jones, N. Voulvoulis, J.N. Lester, Human pharmaceuticals in wastewater treatment processes, Crit. Rev. Environ. Sci. Technol., 35 (2005) 401–427.
[11] M.B. Ahmed, J.L. Zhou, H.H. Ngo, W. Guo, Adsorptive removal of antibiotics from water and wastewater: Progress and challenges, Sci. Total Environ., 532 (2015) 112–126.
[12] L.E. Brus, Electron–electron and electron-hole interactions in small semiconductor crystallites: The size dependence of the lowest excited electronic state, J. Chem. Phys., 80 (1984) 4403–4409.
[13] S. Chen, W. Liu, Characterization and antiwear ability of non-coated zns nanoparticles and ddp-coated zns nanoparticles, Mater. Res. Bull., 36 (2001) 137–143.
[14] N. Hebalkar, A. Lobo, S.R. Sainkar, S.D. Pradhan, W. Vogel, J. Urban, S.K. Kulkarni, Properties of zinc sulphide nanoparticles stabilized in silica, J. Mater. Sci., 36 (2001) 4377–4384.
[15] C. Sombuthawee, S.B. Bonsall, F.A. Hummel, Phase equilibria in the systems zns-mns, zns-cuins2, and mns-cuins2, J. Solid State Chem., 25 (1978) 391–399.

[16] X. Zhou, T. Shi, H. Zhou, Hydrothermal preparation of zno-reduced graphene oxide hybrid with high performance in photocatalytic degradation, Appl. Surf. Sci., 258 (2012) 6204–6211.

[17] G. Wang, J. Yang, J. Park, X. Gou, B. Wang, H. Liu, J. Yao, Facile synthesis and characterization of graphene nanosheets, J. Phys. Chem. C., 112 (2008) 8192–8195.

[18] M. Sookhakian, Y.M. Amin, W.J. Basirun, Hierarchically ordered macro-mesoporous zns microsphere with reduced graphene oxide supporter for a highly efficient photodegradation of methylene blue, Appl. Surf. Sci., 283 (2013) 668–677.

[19] M. Sookhakian, Y.M. Amin, W.J. Basirun, M.T. Tajabadi, N. Kamarulzaman, Synthesis, structural, and optical properties of type-ii zno–zns core–shell nanostructure, J. Lumin., 145 (2014) 244–252.

[20] A. Fakhri, S. Adami, Adsorption and thermodynamic study of cephalosporins antibiotics from aqueous solution onto mgo nanoparticles, J. Taiwan Inst. Chem. Eng., 45 (2014) 1001–1006.

[21] E. Martınez-Flores, J. Negrete, G. Torres Villaseñor, Structure and properties of zn–al–cu alloy reinforced with alumina particles, Mater. Des., 24 (2003) 281–286.

[22] A. Fakhri, Investigation of mercury (ii) adsorption from aqueous solution onto copper oxide nanoparticles: Optimization using response surface methodology, Process Saf. Environ., 93 (2015) 1–8.

[23] A. Fakhri, Application of response surface methodology to optimize the process variables for fluoride ion removal using maghemite nanoparticles, J. Saudi Chem. Soc., 18 (2014) 340–347.

[24] M.J. Tempkin, V. Pyzhev, Kinetics of ammonia synthesis on promoted iron catalysts, Acta Physicochim. URS., 12 (1940) 217–222.

[25] Y.S. Ho, Citation review of lagergren kinetic rate equation on adsorption reactions, Scientometrics, 59 (2004) 171–177.

[26] R. Djeribi, O. Hamdaoui, Sorption of copper(ii) from aqueous solutions by cedar sawdust and crushed brick, Desalination, 225 (2008) 95–112.

[27] S. Basha, Z.V.P. Murthy, B. Jha, Sorption of hg(ii) onto carica papaya: Experimental studies and design of batch sorber, Chem. Eng. J., 147 (2009) 226–234.

[28] A. Chatterjee, S. Schiewer, Multi-resistance kinetic models for biosorption of cd by raw and immobilized citrus peels in batch and packed-bed columns, Chem. Eng. J., 244 (2014) 105–116.

[29] T. Fan, Y. Liu, B. Feng, G. Zeng, C. Yang, M. Zhou, H. Zhou, Z. Tan, X. Wang, Biosorption of cadmium(ii), zinc(ii) and lead(ii) by penicillium simplicissimum: Isotherms, kinetics and thermodynamics, J. Hazard. Mater., 160 (2008) 655–661.

[30] H. Lalhruaitluanga, K. Jayaram, M.N.V. Prasad, K.K. Kumar, Lead(ii) adsorption from aqueous solutions by raw and activated charcoals of melocanna baccifera roxburgh (bamboo)—a comparative study, J. Hazard. Mater., 175 (2010) 311–318.

[31] X. Zhang, X. Wang, Adsorption and desorption of nickel(ii) ions from aqueous solution by a lignocellulose/montmorillonite nanocomposite, PLoS ONE, 10 (2015) e0117077.